PHYSICAL REVIEW B **86**, 064401 (2012)

Tensor network states and ground-state fidelity for quantum spin ladders

Sheng-Hao Li, Qian-Qian Shi, Yao-Heng Su, Jin-Hua Liu, Yan-Wei Dai, and Huan-Qiang Zhou
Centre for Modern Physics and Department of Physics, Chongqing University, Chongqing 400044, The People's Republic of China

(Received 27 February 2012; revised manuscript received 6 June 2012; published 1 August 2012)

We have developed an efficient tensor network algorithm for spin ladders, which generates ground-state wave functions for infinite-size quantum spin ladders. The algorithm is able to efficiently compute the ground-state fidelity per lattice site, a universal phase transition marker, thus offering a powerful tool to unveil quantum many-body physics underlying spin ladders. To illustrate our scheme, we consider the two-leg and three-leg Heisenberg spin ladders with staggering dimerization, the two-leg Heisenberg spin ladder with cyclic four-spin exchange, and the ferromagnetic frustrated two-leg ladder. The ground-state phase diagrams thus yielded are reliable, compared with the previous studies based on the the exact diagonalization and the density matrix renormalization group. Our results indicate that the ground-state fidelity per lattice site successfully captures quantum criticalities in spin ladders.

DOI: 10.1103/PhysRevB.86.064401 PACS number(s): 74.20.−z, 02.70.−c, 71.10.Fd

I. INTRODUCTION

Recently, tensor networks (TNs) provide a convenient means to represent quantum wave functions in classical simulations of quantum many-body lattice systems, such as the matrix product states (MPSs)[1–5] in one spatial dimension and the projected entangled-pair states (PEPSs)[6–8] in two and higher spatial dimensions. The development of various numerical algorithms in the context of the TN representations has led to significant advances in our understanding of quantum many-body lattice systems in both one and two spatial dimensions.[3–17] A remarkable aspect of these advances is relevant to a fidelity approach to critical phenomena in quantum many-body physics, which has emerged as a consequence of the fact that fidelity, a basic notion in quantum information science, is a measure of quantum state distinguishability. The approach allows us to characterize critical phenomena in a variety of quantum many-body lattice systems in any spatial dimensions.[18–27] As argued in Refs. 18–23, the ground-state fidelity per lattice site is able to capture drastic changes of the ground-state wave functions around a phase transition point. This, in combination with the fact that many powerful numerical algorithms have been developed in the context of the TN representation, provides a powerful means to unveil quantum criticality underlying quantum many-body systems. In fact, a systematic scheme to study critical phenomena in quantum many-body lattice systems consists of three steps, as advocated in Ref. 28: First, map out the ground-state phase diagram by computing the ground-state fidelity per lattice site; second, derive local order parameters (if any) from the reduced density matrices for a representative ground-state wave function in a given phase; third, characterize any phase without any long range order.

In the last decades, low-dimensional quantum spin systems, such as spin ladders, have been the subject of extensive experimental and theoretical interest.[29,30] Many fascinating features of the ladder systems have long been understood theoretically from both analytical and numerical approaches.[31–58] Among them is an intriguing property that the existence of an excitation gap depends on the number of legs: spin excitations are gapful for an even-leg Heisenberg spin ladder and gapless for an odd-leg Heisenberg spin ladder. There are also a number of low-dimensional compounds of transition metals, such as $SrCu_2O_3$ (Ref. 59), $(VO)_2P_2O_7$ (Ref. 60), $La_6Ca_8Cu_{24}O_{41}$ (Ref. 61), and $(C_5H_{12}N)_2CuBr_4$ (Ref. 62), whose properties are well described adequately by multileg spin ladders. Lying between quantum lattice systems in one and two spatial dimensions, spin ladders often exhibit some attractive behaviors, due to their rich critical properties. Given the importance of spin-ladder systems in condensed-matter physics, it is somewhat surprising that no efforts have been made to develop any efficient algorithm in the context of the TN representations, which enables us to efficiently compute the ground-state fidelity per lattice site.

This paper aims to fill in this gap. We develop an algorithm to generate efficiently ground-state wave functions for infinite-size spin ladders. The two-leg and three-leg Heisenberg spin ladders with staggering dimerization, the two-leg Heisenberg spin ladder with cyclic four-spin exchange, and the ferromagnetic frustrated two-leg ladder are investigated. First, for the two-leg spin ladder with staggering dimerization, it yields very accurate values of the ground-state energy per site, with the accuracy reaching up to 10^{-4} already for the truncation dimension up to 6. Then we evaluate the ground-state fidelity per lattice site to identify critical points. The simulation results for all four spin ladders are in good agreement with the previous studies[31–42] based on the exact diagonalization and/or the density matrix renormalization group (DMRG).[63] Therefore, the TN algorithm provides an efficient means to evaluate the ground-state fidelity per lattice site, which in turn successfully captures quantum criticalities in spin ladders.

The layout of the paper is as follows. In Sec. II, we develop an efficient algorithm based on the TN representation suitable to describe a ground-state wave function for an infinite-size spin ladder, which is the adaptation of the infinite PEPS representation to a spin ladder. In Sec. III, an efficient way to evaluate the ground-state fidelity per lattice site is described in the TN representation. In Sec. IV, we present our simulation results for four infinite-size spin-ladder systems: the two-leg and three-leg Heisenberg spin ladders with staggering dimerization, the two-leg Heisenberg spin ladder with cyclic four-spin exchange, and the ferromagnetic frustrated two-leg ladder. Section V is devoted to a summary.

II. TENSOR NETWORK REPRESENTATION FOR SPIN LADDERS

Let us describe the TN representation suitable to describe a ground-state wave function for an infinite-size spin ladder. Actually, the TN is a particular case of the PEPS[6] adapted to the geometry of an infinite-size spin-ladder system. Suppose the Hamiltonian is translationally invariant under shifts by either one or two lattice sites along the legs: $H = \sum_{\langle i,\alpha\rangle} h_{\langle i,\alpha\rangle}$, with the $\langle i,\alpha\rangle$th plaquette Hamiltonian density $h_{\langle i,\alpha\rangle}$ acting on sites i and $(i+1)$ along the αth and $(\alpha+1)$th legs. Here, $\langle i,\alpha\rangle$ runs over all the possible plaquettes by taking $i \in \{-\infty,\ldots,+\infty\}$, and $\alpha = 1,\ldots,n-1$, with n being the number of the legs. Assume that the TN representation for a wave function enjoys the translational invariance under shifts by two lattice sites along the legs. In the following, we focus on a detailed description for a two-leg spin ladder, with a brief discussion for an n-leg ladder system.

For an infinite-size two-leg spin-ladder system, we need only four different four-index tensors, $A^s_{\ell rd}$, $B^s_{\ell rd}$, $C^s_{\ell ru}$, and $D^s_{\ell ru}$, to store the wave function.[64] Here, $A^s_{\ell rd}$, $B^s_{\ell rd}$, $C^s_{\ell ru}$, and $D^s_{\ell ru}$ are made of complex numbers labeled by one physical index s and four inner bond indices ℓ, r, u, and d, where $s = 1,\ldots,\mathbb{d}$, with $\mathbb{d}$ being the dimension of the local Hilbert space, and $\ell, r, u, d = 1,\ldots,\mathbb{D}$, with $\mathbb{D}$ being the bond dimension. A four-index tensor $A^s_{\ell rd}$ is visualized in Fig. 1(i), with a similar pictorial representation for the tensors $B^s_{\ell rd}$, $C^s_{\ell ru}$, and $D^s_{\ell ru}$. A TN representation for the ground-state wave function is shown for an infinite-size two-leg spin ladder in Fig. 1(ii). There are two different but equivalent choices of the unit cell for such an infinite-size TN: One is chosen as A, B, D, and C clockwise if i is even; the other is chosen as B, A, C, and D clockwise if i is odd [see Fig. 1(iii)].

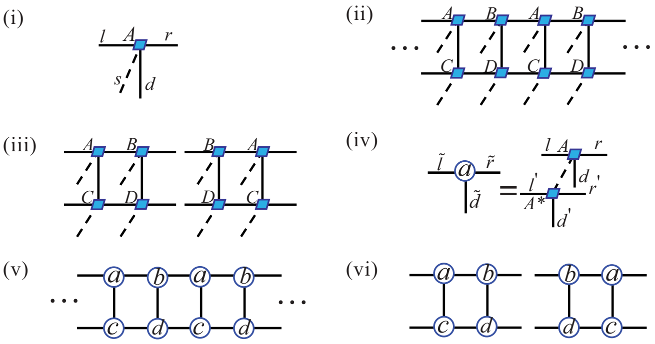

FIG. 1. (Color online) (i) Four-index tensor A^s_{lrd} used to represent a TN representation for the ground-state wave function for an infinite-size two-leg spin ladder, with s being a physical index, l, r, and d denoting the inner indices. (ii) Pictorial representation for a TN state $|\psi\rangle$ with leg and rung bonds, which are used to absorb an operator acting on the ith plaquette. (iii) Two different choices of the unit cell for an infinite-size TN state, made of four four-index tensors A, B, C, and D. (iv) A double tensor $a_{\tilde{\ell}\tilde{r}\tilde{d}}$ is formed from the four-index tensor $A^s_{\ell rd}$ and its complex conjugate $(A^*)^s_{\ell' r' d'}$, with $\tilde{\ell} \equiv (\ell,\ell')$, $\tilde{r} \equiv (r,r')$, and $\tilde{d} \equiv (d,d')$. (v) The TN representation for the norm of a ground-state wave function in an infinite-size spin ladder. (vi) Two different choices of the unit cells for the norm TN, consisting of four double tensors a, b, c, and d.

Now let us turn to the computation of the norm for a quantum state wave function. To this end, we introduce double tensors $a_{\tilde{\ell}\tilde{r}\tilde{d}}$, $b_{\tilde{\ell}\tilde{r}\tilde{d}}$, $c_{\tilde{\ell}\tilde{r}\tilde{u}}$, and $d_{\tilde{\ell}\tilde{r}\tilde{u}}$, with $\tilde{\ell} \equiv (\ell,\ell')$, $\tilde{r} \equiv (r,r')$, $\tilde{u} \equiv (u,u')$, and $\tilde{d} \equiv (d,d')$. They form from the four-index tensors $A^s_{\ell rd}$, $B^s_{\ell rd}$, $C^s_{\ell ru}$, and $D^s_{\ell ru}$, and their complex conjugates; see Fig. 1(iv) for a pictorial representation of the double tensors. With these double tensors, the TN for the norm of a wave function is shown in Fig. 1(v). Again, we have two different but equivalent choices for the unit cell of the norm TN: One is a, b, d, and c clockwise if i is even; the other is b, a, c, and d clockwise if i is odd [see Fig. 1(vi)].

The expectation value of an operator acting on a plaquette, such as the ground-state energy per unit cell, also admits a TN representation, which absorbs the operator acting on a plaquette for an infinite-size spin-ladder system. For a randomly chosen initial state $|\psi_0\rangle$, the energy is expressed as

$$E_g = \frac{\langle\psi_0|H|\psi_0\rangle}{\langle\psi_0|\psi_0\rangle}. \tag{1}$$

For different choices of the unit cell, we get two different but equivalent forms of the zero-dimensional transfer matrix E constructed from four double tensors $a_{\tilde{\ell}\tilde{r}\tilde{d}}$, $b_{\tilde{\ell}\tilde{r}\tilde{d}}$, $d_{\tilde{\ell}\tilde{r}\tilde{u}}$, and $c_{\tilde{\ell}\tilde{r}\tilde{u}}$, one of which is shown in Fig. 2(i). The dominant left and right eigenvectors of the transfer matrix E constitute the environment tensors, visualized in Fig. 2(ii). This enables us to absorb an operator acting on the ith plaquette A, B, D, and C clockwise, if i is even, as shown in Fig. 2(iii), and compute the energy per unit cell, as shown in Fig. 2(iv). The same procedure may be used to compute the energy per unit cell for an operator acting on the ith plaquette B, A, C, and D clockwise, if i is odd.

To update the TN representation, we compute the energy gradient with respect to four-index tensors:

$$\frac{\partial E_g}{\partial A^s_{\ell rd}} = \frac{\partial\langle\psi_0|H|\psi_0\rangle/\partial A^s_{\ell rd}}{\langle\psi_0|\psi_0\rangle} - E_g \cdot \frac{\partial\langle\psi_0|\psi_0\rangle/\partial A^s_{\ell rd}}{\langle\psi_0|\psi_0\rangle}. \tag{2}$$

Here, a four-index tensor $A^s_{\ell rd}$ is used to explain how to efficiently evaluate the energy gradient in the context of the TN representation for an infinite-size two-leg spin ladder, with the details visualized in Fig. 3. Notice that the contributions to the

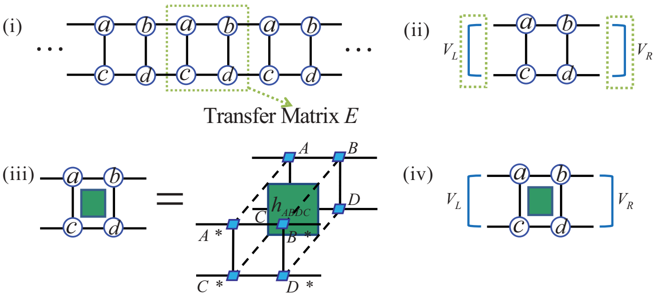

FIG. 2. (Color online) (i) The transfer matrix E for an infinite-size norm TN, which is constructed from four double tensors $a_{\tilde{\ell}\tilde{r}\tilde{d}}$, $b_{\tilde{\ell}\tilde{r}\tilde{d}}$, $c_{\tilde{\ell}\tilde{r}\tilde{u}}$, and $d_{\tilde{\ell}\tilde{r}\tilde{u}}$, with $\tilde{\ell} \equiv (\ell,\ell')$, $\tilde{r} \equiv (r,r')$, $\tilde{u} \equiv (u,u')$, and $\tilde{d} \equiv (d,d')$. (ii) The dominant left and right eigenvectors V_L and V_R of the transfer matrix E. (iii) A unit cell with the Hamiltonian density h_{ABDC} acted on the plaquette. (iv) The ground-state energy per unit cell is computed from the eigenvectors V_L, V_R and four four-index tensors $A^s_{\ell rd}$, $B^s_{\ell rd}$, $C^s_{\ell ru}$, and $D^s_{\ell ru}$.

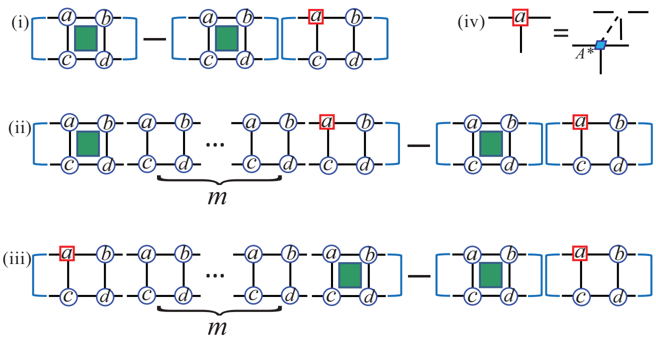

FIG. 3. (Color online) The contribution to the energy gradient for an infinite-size spin ladder consists of three parts (for a given choice of a plaquette on which the Hamiltonian acts on): (i) the hole cell with the tensor $A^s_{\ell rd}$ removed and the Hamiltonian cell with the Hamiltonian density acting on a plaquette locate on the same cell; (ii) the hole cell locates on the right-hand side of the Hamiltonian cell; (iii) the hole cell locates on the left-hand side of the Hamiltonian cell. In the latter two cases, there are m cells between the hole and Hamiltonian cells, where $m \in (0,1,2,3,\dots)$. Here, the hole cell is visualized in (iv), with the tensor $A^s_{\ell rd}$ removed. Note that only the contribution from the plaquette "*abdc*", as labeled here, is visualized. However, there is also a contribution from the plaquette "*bacd*".

energy gradient come from three parts (for a given choice of a plaquette on which the Hamiltonian acts on): (i) the hole cell with the four-index tensor $A^s_{\ell rd}$ absent and the Hamiltonian cell with the Hamiltonian density sandwiched locate on the same cell; (ii) the hole cell locates on the right-hand side of the Hamiltonian cell; (iii) the hole cell locates on the left-hand side of the Hamiltonian cell. In both cases (ii) and (iii), there are m cells between the hole cell and the Hamiltonian cell, where $m \in (0,1,2,3,\dots)$. We stress that the contributions from both plaquettes "*abdc*" and "*bacd*" to the energy gradient should be summed up. As such, the four-index tensor $A^s_{\ell rd}$ is updated as follows:

$$A^s_{\ell rd} = A^s_{\ell rd} - \delta \, \frac{\partial E_g/\partial A^s_{\ell rd}}{\max_{(\ell,r,d)} \left|\partial E_g/\partial A^s_{\ell rd}\right|}, \tag{3}$$

where δ denotes the step size during updating. We stress that, for a two-leg spin ladder, we should update four different four-index tensors $A^s_{\ell rd}$, $B^s_{\ell rd}$, $C^s_{\ell ru}$, and $D^s_{\ell ru}$ simultaneously. Here, it is proper to point out that our updating procedure is closely connected to the infinite PEPS algorithm[8] and the translationally invariant MPS algorithm.[11]

The above updating procedure yields new tensors $A^s_{\ell rd}$, $B^s_{\ell rd}$, $C^s_{\ell ru}$, and $D^s_{\ell ru}$ for a two-leg spin ladder. Repeating this procedure until the ground-state energy per unit cell converges, we anticipate that the system's ground-state wave function is generated in the TN representation. In our implementation, the initial value of δ is chosen to be any value between 0 and 1. Actually, there are different ways to choose δ in order to get a reliable ground-state wave function. Specifically, δ is reduced gradually up to 10^{-6}, until the energy reaches a fixed point within a preset error tolerance. We find that the simulation results are insensitive to either a chosen initial value of δ or the way how to reduce it. The computation cost scales as $\mathbb{D}^6$, since the truncation dimensions along rungs and legs are chosen to be the same. However, one of the advantages of the algorithm is that they may take different values.

For a three-leg spin ladder, one should introduce four different four-index tensers $A^s_{\ell rd}$, $B^s_{\ell rd}$, $E^s_{\ell ru}$, and $F^s_{\ell ru}$, and two different five-index tensers $C^s_{\ell rud}$ and $D^s_{\ell rud}$. In this case, the computation cost scales as $\mathbb{D}^9$, if the truncation dimensions along rungs and legs are chosen to be the same. Similarly, more tensors are needed for a multileg spin ladder. However, the algorithm is applicable to a multileg spin ladder, as long as the memory is sufficient to store the TN tensors. Although the computational cost with $\mathbb{D}$ remains the same for a multileg spin ladder, the cost is, roughly speaking, linearly increasing with the increasing number of the tensors in the unit cell.

III. THE GROUND-STATE FIDELITY PER LATTICE SITE

For a spin-ladder system, we assume h is a control parameter. For two different ground states, $|\psi(h_1)\rangle$ and $|\psi(h_2)\rangle$, corresponding to two different values h_1 and h_2 of the control parameter h, the ground-state fidelity $F(h_1,h_2) = |\langle\psi(h_2)|\psi(h_1)\rangle|$ asymptotically scales as $F(h_1,h_2) \sim d(h_1,h_2)^N$, with N the total number of the lattice sites. Here, $d(h_1,h_2)$ is the scaling parameter, introduced in Refs. 18–20 for one-dimensional quantum lattice systems and in Refs. 21 for two- and higher-dimensional quantum lattice systems. In fact, $d(h_1,h_2)$ characterizes how fast the fidelity goes to zero when the thermodynamic limit is approached. Physically, the scaling parameter $d(h_1,h_2)$ is the averaged fidelity per lattice site,

$$\ln d(h_1,h_2) \equiv \lim_{N\to\infty} \frac{\ln F(h_1,h_2)}{N}, \tag{4}$$

which is well defined in the thermodynamic limit even if $F(h_1,h_2)$ becomes trivially zero. It satisfies the properties inherited from the fidelity $F(h_1,h_2)$: (i) normalization $d(h,h) = 1$; (ii) symmetry $d(h_1,h_2) = d(h_2,h_1)$; and (iii) range $0 \leqslant d(h_1,h_2) \leqslant 1$.

Suppose a ground-state wave function has been generated from the TN algorithm for a given value of h; one needs to figure out an efficient way to evaluate the ground-state fidelity per lattice site $d(h_1,h_2)$, a universal marker to detect quantum criticalities: A phase transition point is characterized by a pinch point on the fidelity surface, which is defined as a function of both h_1 and h_2. In Figs. 4(i) and 4(ii), we have visualized two ground-state wave functions $|\psi(h_1)\rangle$ and $|\psi(h_2)\rangle$. In Fig. 4(iii), a double tensor $a'_{\tilde\ell\tilde r\tilde d}(h_1,h_2)$, with $\tilde\ell \equiv (\ell,\ell')$, $\tilde r \equiv (r,r')$, and $\tilde d \equiv (d,d')$, is defined, which is formed from the four-index tensor $A^s_{\ell rd}(h_1)$ and the complex conjugate of the four-index tensor $A^s_{\ell rd}(h_2)$. Then, a pictorial representation of the ground-state fidelity $F(h_1,h_2)$ is shown in Fig. 4(iv), where the fidelity transfer matrix E' is defined for an infinite-size fidelity TN. Therefore, the ground-state fidelity per lattice site $d(h_1,h_2)$ between two different states $|\psi(h_1)\rangle$ and $|\psi(h_2)\rangle$ is obtained by computing the dominant eigenvalue λ_1 of the transfer matrix E', as shown in Fig. 4(v). Indeed, we have $d(h_1,h_2) = |\lambda_1^{1/4}|$ for our choice of the unit cell. The same procedure also works for a multileg spin ladder.

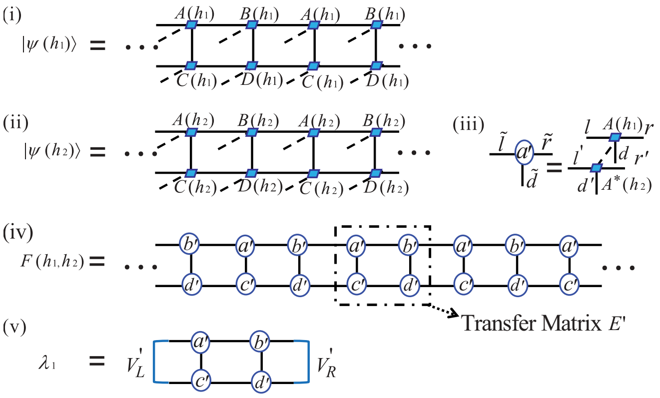

FIG. 4. (Color online) The pictorial representations for the fidelity $F(h_1,h_2)$ and the fidelity per lattice site $d(h_1,h_2)$ between two different ground states, $|\psi(h_1)\rangle$ and $|\psi(h_2)\rangle$, with h_1 and h_2 being two different values of the control parameter h, for an infinite-size two-leg spin ladder. (i) A ground-state wave function $|\psi(h_1)\rangle$ in the TN representation, which is translationally invariant under two-site shifts, with the control parameter $h = h_1$. Here, $A^s_{\ell rd}(h_1)$, $B^s_{\ell rd}(h_1)$, $C^s_{\ell ru}(h_1)$, and $D^s_{\ell ru}(h_1)$ are the constituent tensors for the ground-state wave function $|\psi(h_1)\rangle$. (ii) Another ground state $|\psi(h_2)\rangle$ in the TN representation, with the control parameter $h = h_2$. Here, $A^s_{\ell rd}(h_2)$, $B^s_{\ell rd}(h_2)$, $C^s_{\ell ru}(h_2)$, and $D^s_{\ell ru}(h_2)$ are the constituent tensors for the ground-state wave function $|\psi(h_2)\rangle$. (iii) A double tensor $a'_{\tilde\ell\tilde r\tilde d}(h_1,h_2)$, with $\tilde\ell \equiv (\ell,\ell')$, $\tilde r \equiv (r,r')$ and $\tilde d \equiv (d,d')$, is formed from the four-index tensor $A^s_{\ell rd}(h_1)$ and the complex conjugate of the four-index tensor $A^s_{\ell rd}(h_2)$. (iv) The TN representation for the ground-state fidelity $F(h_1,h_2)$ between two different ground states, $|\psi(h_1)\rangle$ and $|\psi(h_2)\rangle$, for an infinite-size two-leg spin ladder. Here, the transfer matrix E' for the infinite-size fidelity TN is constructed from four double tensors $a'_{\tilde\ell\tilde r\tilde d}(h_1,h_2)$, $b'_{\tilde\ell\tilde r\tilde d}(h_1,h_2)$, $c'_{\tilde\ell\tilde r\tilde u}(h_1,h_2)$, and $d'_{\tilde\ell\tilde r\tilde u}(h_1,h_2)$. (v) The ground-state fidelity per lattice site $d(h_1,h_2)$ is obtained by computing the dominant eigenvalue λ_1 of the fidelity transfer matrix E', with V'_L and V'_R being the left and right dominant eigenvectors. As such, we have $d(h_1,h_2) = |\lambda_1^{1/4}|$.

IV. THE MODELS AND SIMULATION RESULTS

As an illustration, we test the algorithm on four different infinite-size spin-ladder systems: the two-leg and three-leg Heisenberg spin ladders with staggering dimerization, the two-leg Heisenberg spin ladder with cyclic four-spin exchange, and the ferromagnetic frustrated two-leg ladder.

A. Two-leg Heisenberg spin ladder

The two-leg Heisenberg spin ladder is described by the Hamiltonian

$$H = \sum_{\alpha=1,2}\sum_{i} J_{\alpha,i} S_{\alpha,i}\cdot S_{\alpha,i+1} + J_\perp \sum_{i} S_{1,i}\cdot S_{2,i}. \qquad (5)$$

Here, $J_{\alpha,i}$ is the interaction coupling along each leg $\alpha = 1,2$, and $J_\perp$ is the interaction along the rungs. To test the TN algorithm, we choose the exchange interaction coupling $J_\perp \in 0.2,0.4,0.6,0.8,1.0$. In addition, $J_{\alpha,i} = J$ if $i+\alpha$ is odd and $J_{\alpha,i} = J'$ if $i+\alpha$ is even, with $J = 1$ and $J' = 0,0.2,0.4,0.6,0.8$, and 1.0.

In Table I, we list our simulation results for the ground-state energy per site, for different values of $J_\perp$ and J', with the truncation dimension up to 6, against the infinite-size ground-state energy per site from the extrapolated exact diagonalization using the symmetric group approach (SGA) in Ref. 31. The fact that they matches very well demonstrates that the TN algorithm is reliable to yield very accurate ground-state wave functions for spin ladders. Specifically, the accuracy for the ground-state energy per site reaches up to 10^{-4} already for such a small value of the truncation dimension.

Let us also compare the ground-state energies from our TN algorithm with the corresponding ground-state energies from the DMRG,[65] for $J_\perp = 0,0.2,0.4,0.6,0.8,1.0$ and $J' = 1.0$. Our results with the truncation dimension $\mathbb{D} = 6$ outperform those from the DMRG. Especially, the improvement is significant for small $J_\perp$'s. For instance, our ground-state energy is lower than that from the DMRG, up to 1%, for $J_\perp = 0$, indicating that very accurate ground-state wave functions are yielded from our TN algorithm. Actually, further increasing the truncation dimension $\mathbb{D}$, more accurate ground-state energies are anticipated.

TABLE I. Comparison between the ground state energies per site from the symmetric-group approach (SGA) in Ref. 31 and our TN algorithm for the infinite-size two-leg Heisenberg ladder. Here, the data from the SGA are the extrapolated value from finite-size counterparts.

$J_\perp$	J'	SGA	Tensor network
0.2	0.0	− 0.376 974 493 6	− 0.376 974
	0.2	− 0.379 293 24	− 0.379 293
	0.4	− 0.386 139	− 0.386 139
	0.6	− 0.39850	− 0.398 509
	0.8	− 0.4181	− 0.418 215
	1.0	− 0.4516	− 0.451 554
0.4	0.0	− 0.383 356 250 2	− 0.383 356
	0.2	− 0.386 802 1	− 0.386 801
	0.4	− 0.395 15	− 0.395 154
	0.6	− 0.4096	− 0.409 689
	0.8	− 0.4334	− 0.432 975
	1.0	− 0.4712	− 0.471 242
0.6	0.0	− 0.395 048 41	− 0.395 048
	0.2	− 0.400 60	− 0.400 597
	0.4	− 0.4117	− 0.411 752
	0.6	− 0.4304	− 0.430 514
	0.8	− 0.4617	− 0.461 940
	1.0	− 0.4994	− 0.499 637
0.8	0.0	− 0.413 56	− 0.413 564
	0.2	− 0.4226	− 0.422 680
	0.4	− 0.4397	− 0.439 913
	0.6	− 0.4674	− 0.467 553
	0.8	− 0.4995	− 0.499 617
	1.0	− 0.5354	− 0.535 502
1.0	0.0	− 0.443 141 384 5	− 0.443 063
	0.2	− 0.4629	− 0.463 080
	0.4	− 0.4870	− 0.487 120
	0.6	− 0.5143	− 0.514 348
	0.8	− 0.5446	− 0.544 634
	1.0	− 0.578 003 409 9	− 0.578 035

Now we turn to a quantum critical point, at which the ladder system undergoes a phase transition, with the staggered dimerization $J_{\alpha,i} = J[1 + (-1)^{i+\alpha}\Delta]$, $\alpha = 1,2$. Here, we fix $\Delta = 0.5$, with the coupling constant J to be unity ($J = 1$), and the exchange interaction coupling constant $J_\perp$ to be a control parameter. To this end, we compute the fidelity per lattice site. In Fig. 5, the ground-state fidelity per lattice site is plotted for the two-leg Heisenberg spin-$\frac{1}{2}$ ladder with staggering dimerization. A two-dimensional fidelity surface embedded in a three-dimensional Euclidean space is shown in the top panel, with a pinch point at (1.24,1.24), implying that a continuous phase transition occurs at $J_{\perp c} \simeq 1.24$. In the bottom panel, a contour plot is shown for the fidelity per lattice site on the $(J_{\perp 1}, J_{\perp 2})$ plane. We stress that no significant shifts are observed for the pinch point, when the truncation dimension is increased up to 6. Therefore, we conclude that a continuous phase transition takes place at $J_{\perp c} \simeq 1.24$, which is very close to earlier results from the mean-field theory,[32] exact diagonalization,[33] and DMRG.[34]

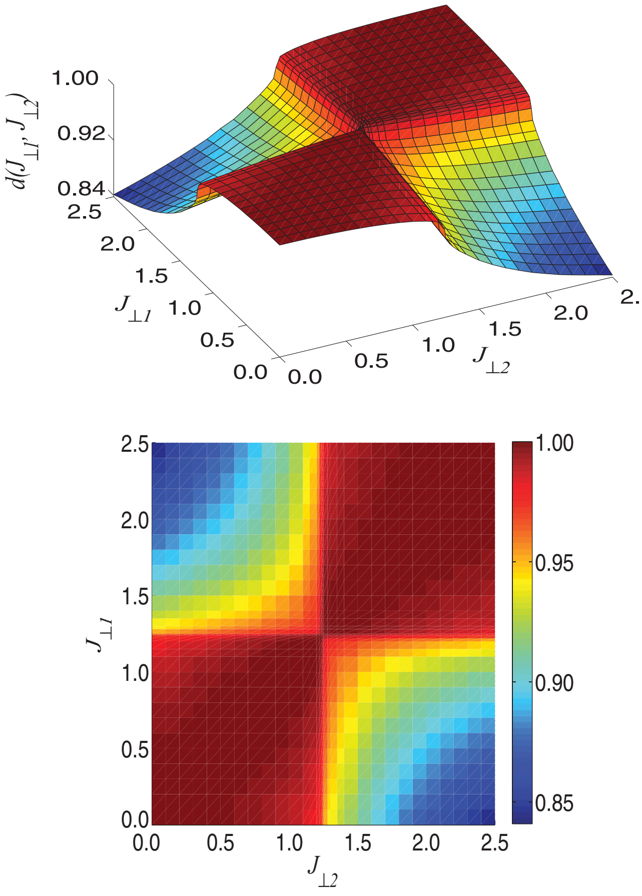

FIG. 5. (Color online) The ground-state fidelity per lattice site $d(J_{\perp 1}, J_{\perp 2})$, as a function of $J_{\perp 1}$ and $J_{\perp 2}$ for the two-leg Heisenberg ladder with staggering dimerization. (Top) A two-dimensional fidelity surface embedded in a three-dimensional Euclidean space. A continuous phase transition point $J_{\perp c} \simeq 1.24$ is identified as a pinch point $(J_{\perp c}, J_{\perp c})$ on the fidelity surface, as argued in Refs. 18–21. Here, we have taken the truncation dimension $\mathbb{D} = 6$. (Bottom) The contour plot of the fidelity per lattice site $d(J_{\perp 1}, J_{\perp 2})$, on the $(J_{\perp 1}, J_{\perp 2})$-plane, for the two-leg Heisenberg ladder with staggering dimerization.

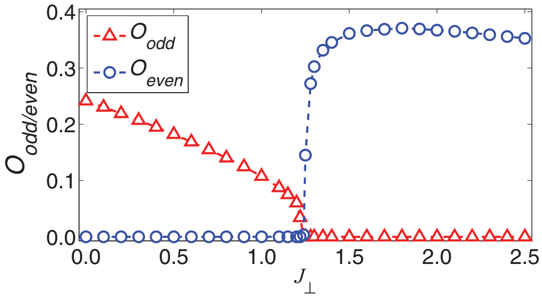

FIG. 6. (Color online) The string order parameters O_{odd}, and O_{even} for the two-leg Heisenberg ladder as a function of $J_\perp$ at $\Delta = 0.5$, respectively. The phase transition takes place at $J_{\perp c} \simeq 1.24$. Here, the truncation dimension is up to 6.

Note that the ground states in the ladder system lack long-rang order in the conventional Landau-Ginzburg sense; thus, there is no local order parameter. Instead, different phases can only be distinguished by a nonlocal string order parameter,[66,67] which is nonzero in one phase and vanishes in the other. The so-called string order parameter was presented by den Nijs and Rommelse.[66] The two distinct string order parameters O_{odd} and O_{even} for two-leg spin ladders are given by

$$O_{\mathrm{odd/even}} = -\lim_{|i-j|\to\infty}\left\langle S^z_{o/e,i}\exp\left\{i\pi\sum_{l=i+1}^{j-1} S^z_{o/e,l}\right\} S^z_{o/e,j}\right\rangle. \tag{6}$$

Here, the composite spin operators are defined as $S^z_{o,i} \equiv S^z_{1,i} + S^z_{2,i}$ and $S^z_{e,i} \equiv S^z_{1,i} + S^z_{2,i+1}$. We calculate the odd and even string order parameters for the z-component spins. For a ladder system with no local order parameter, it turns out that the intersection of the curves of two distinct string order parameters implies a phase transition point.

In Fig. 6, we plot the odd and even string order parameters O_{odd}, and O_{even} for the two-leg Heisenberg spin-$\frac{1}{2}$ ladder with staggering dimerization $\Delta = 0.5$. For the interaction coupling constant $J_\perp < 1.24$ with $\Delta = 0.5$, one has $O_{\mathrm{odd}} \neq 0$ and $O_{\mathrm{even}} = 0$, implying the leg-dimer phase; while $O_{\mathrm{odd}} = 0$ and $O_{\mathrm{even}} \neq 0$ for the interaction coupling constant $J_\perp > 1.24$, with $\Delta = 0.5$, implying the rung-dimer phase. Indeed, $O_{\mathrm{odd}} = 0$ and $O_{\mathrm{even}} = 0$ for the interaction coupling constant $J_\perp \simeq 1.24$ with $\Delta = 0.5$; thus, the phase transition takes place at $J_{\perp c} \simeq 1.24$. Our results for the string order parameters are in a good agreement with the previous studies from the exact diagonalization.[33] We stress that no significant shifts are observed for the phase transition point, which is fixed at $J_{\perp c} \simeq 1.24$ when the truncation dimension is increased up to 6. The critical point thus determined is identical to that from the fidelity per site approach.

B. Three-leg Heisenberg spin ladder

The three-leg Heisenberg spin ladder is described by the Hamiltonian

$$\begin{aligned} H = {} & \sum_{\alpha=1,2,3}\sum_i J_{\alpha,i}\,\mathbf{S}_{\alpha,i}\cdot\mathbf{S}_{\alpha,i+1} \\ & + J_\perp \sum_i (\mathbf{S}_{1,i}\cdot\mathbf{S}_{2,i} + \mathbf{S}_{2,i}\cdot\mathbf{S}_{3,i}). \end{aligned} \tag{7}$$

For the three-leg Heisenberg spin ladder with the staggered dimerization, the exchange interaction coupling along the αth leg takes the form $J_{\alpha,i} = J[1+(-1)^{i+\alpha}\Delta]$. To capture quantum criticality in the three-leg ladder, we compute the ground-state fidelity per site by fixing $\Delta = 0.5$, and $J = 1$, with the exchange interaction coupling constant $J_\perp$ as a control parameter. In Fig. 7, we plot a two-dimensional fidelity surface embedded in a three-dimensional Euclidean space, namely, the ground-state fidelity per lattice site $d(J_{\perp 1}, J_{\perp 2})$ as a function of $J_{\perp 1}$ and $J_{\perp 2}$, for the three-leg Heisenberg spin-$\frac{1}{2}$ ladder with staggering dimerization. It yields reliable results, with only the truncation dimension up to 6. A continuous phase transition point $J_{\perp c} \simeq 0.96$ is identified as a pinch point $(J_{\perp c},\, J_{\perp c})$ on the fidelity surface, consistent with the previous results from the DMRG method.[32,35]

In this spin-ladder system, there is no local order parameter. Different phases can only be distinguished by a nonlocal string order parameter[66,67] O_{odd} and O_{even} in Eq. (6), with the composite spin operators for three-leg ladders defined as $S^z_{o,i} \equiv S^z_{1,i} + S^z_{2,i} + S^z_{3,i}$ and $S^z_{e,i} \equiv S^z_{1,i} + S^z_{2,i+1} + S^z_{3,i+2}$. Given that the ladder system is translationally invariant under two-site shifts along the legs, we have two choices of the unit cell for any odd $j-i$, depending on the locations of the sites on which $S^z_{o,i}$ act. Equivalently, there are also two different choices for any even $j-i$. Here, we restrict ourselves to consider an odd $j-i$. In contrast to the two-leg ladder system, two different choices yield different results for the string order parameters O_{odd} and O_{even} as functions of $J_\perp$, as depicted in the top and bottom panels in Fig. 8. This is due to the fact that, for the two-leg ladder, some symmetry exists to constrain two values arising from two different choices of the unit cell to be the same. In fact, the two-leg ladder is invariant under the combined action of an operation to exchange the left and right legs and the translation under one-site shifts along the legs. In contrast, the three-leg ladder is simply invariant under an operation to exchange the left and right legs, with the middle leg remaining intact. Therefore, there is no operation, which, combined with the one-site shifts along the legs, leaves the three-leg ladder invariant.

For the first choice, $O_{\text{odd}} \neq 0$ and $O_{\text{even}} = 0$ for the interaction coupling constant $J_\perp < 0.96$ and $O_{\text{odd}} = 0$ and $O_{\text{even}} \neq 0$ for the interaction coupling constant $J_\perp > 0.96$. For the second choice, $O_{\text{odd}} = 0$ and $O_{\text{even}} \neq 0$ for $J_\perp < 0.96$ and $O_{\text{even}} = 0$ and $O_{\text{odd}} \neq 0$ for $J_\perp > 0.96$. However, for both choices, it is found that $O_{\text{odd}} = 0$ and $O_{\text{even}} = 0$ for $J_\perp \simeq 0.96$ with $\Delta = 0.5$, implying that the phase transition point is located at $J_{\perp c} \simeq 0.96$. Here, we note that our results for the odd string order parameters corresponding to the first choice are consistent with the previous results from the finite-size

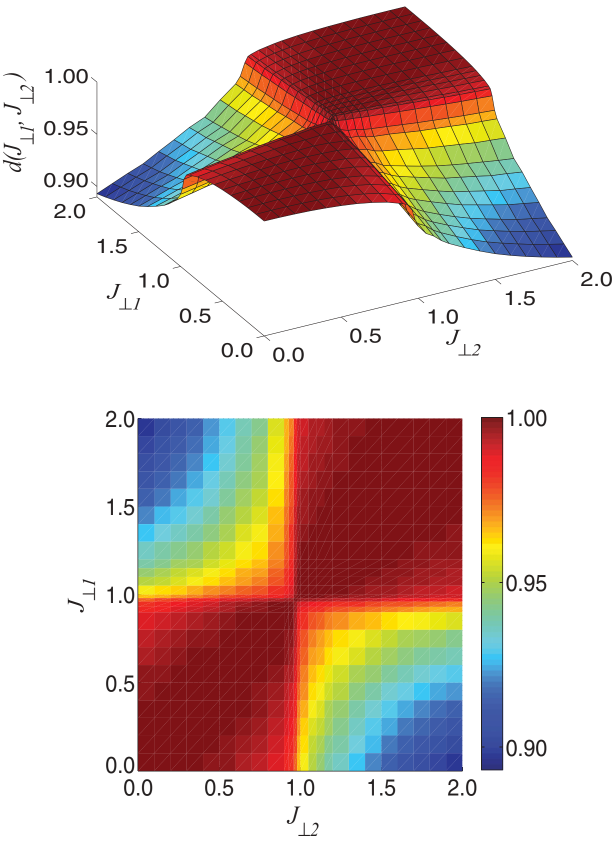

FIG. 7. (Color online) The ground-state fidelity per lattice site $d(J_{\perp 1}, J_{\perp 2})$, as a function of $J_{\perp 1}$ and $J_{\perp 2}$ for the three-leg Heisenberg ladder with staggering dimerization. (Top) A two-dimensional fidelity surface embedded in a three-dimensional Euclidean space. A continuous phase transition point $J_{\perp c} \simeq 0.96$ is identified as a pinch point $(J_{\perp c}, J_{\perp c})$ on the fidelity surface, as argued in Refs. 18–21. Here, we have taken the truncation dimension $\mathbb{D} = 6$. (Bottom) The contour plot of the fidelity per lattice site $d(J_{\perp 1}, J_{\perp 2})$, on the $(J_{\perp 1}, J_{\perp 2})$ plane, for the three-leg Heisenberg ladder with staggering dimerization.

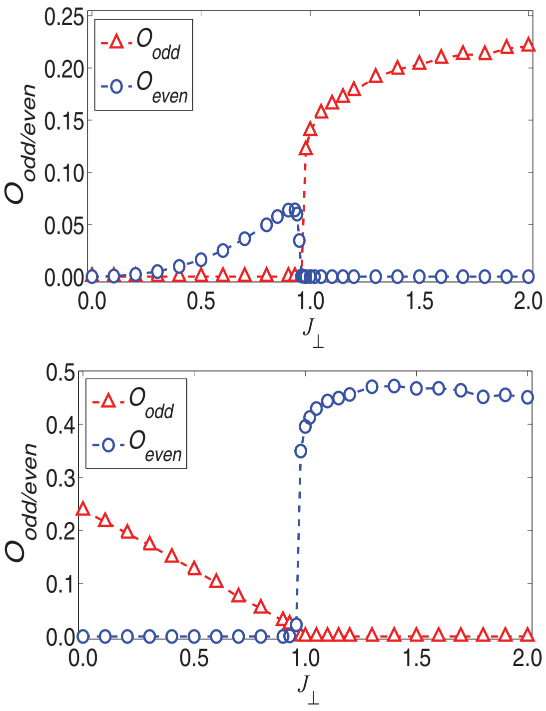

FIG. 8. (Color online) The string order parameters O_{odd} and O_{even} for the three-leg Heisenberg ladder as a function of $J_\perp$ at $\Delta = 0.5$, respectively. Here, the top and the bottom panels correspond to two different choices of the unit cell for the ladder system, which is translationally invariant under shifts by two lattice sites along the legs, respectively. For both choices, the phase transition point is located at $J_{\perp c} \simeq 0.96$. Here, the truncation dimension is up to 6.

DMRG method,[35] and the phase transition point determined is identical to that from the fidelity per site approach.

C. Two-leg Heisenberg spin-$\frac{1}{2}$ ladder with cyclic four-spin exchange

The ladder system is described by the Hamiltonian

$$H = \sum_{\alpha=1,2}\sum_{i} J_{\alpha,i} S_{\alpha,i}\cdot S_{\alpha,i+1} + J_{\perp}\sum_{i} S_{1,i}\cdot S_{2,i} + K\sum_{i}\left(P_{i,i+1}+P^{-1}_{i,i+1}\right). \tag{8}$$

Here, $S_{\alpha,i}$ $(\alpha = 1,2)$ denotes the spin-$\frac{1}{2}$ Pauli operators at site i on the αth leg, $J_{i,\alpha}$ is the intrachain coupling between two neighboring spins in each chain, $J_{\perp}$ is the interchain coupling between two spins on each rung, and K is the cyclic four-spin exchange interaction coupling. The cyclic four-spin permutation operator $P_{i,i+1}$ $(P^{-1}_{i,i+1})$ exchanges the four spins around the ith plaquette as $S_{1,i} \to S_{1,i+1} \to S_{2,i+1} \to S_{2,i} \to S_{1,i}$, which can be decomposed in terms of the Pauli spin operators involving bilinear and biquadratic terms:

$$\begin{aligned} P_{i,i+1} + P^{-1}_{i,i+1} = {} & S_{1,i}\cdot S_{1,i+1} + S_{1,i+1}\cdot S_{2,i+1} + S_{2,i+1}\cdot S_{2,i} \\ & + S_{2,i}\cdot S_{1,i} + S_{1,i}\cdot S_{2,i+1} + S_{1,i+1}\cdot S_{2,i} \\ & + 4(S_{1,i}\cdot S_{1,i+1})(S_{2,i+1}\cdot S_{2,i}) \\ & + 4(S_{2,i}\cdot S_{1,i})(S_{1,i+1}\cdot S_{2,i+1}) \\ & - 4(S_{1,i}\cdot S_{2,i+1})(S_{1,i+1}\cdot S_{2,i}). \end{aligned} \tag{9}$$

Actually, this ladder system has been investigated by the exact diagonalization[42,43] and DMRG.[36–39,42]

For simplicity, we choose $K = \sin\theta$, and $J_{\perp} = J_{\alpha,i} = \cos\theta$, with $\theta \in [-\pi,\pi]$. In Fig. 9, we plot a two-dimensional fidelity surface embedded in a three-dimensional Euclidean space for the two-leg Heisenberg spin-$\frac{1}{2}$ ladder with cyclic four-spin exchange. As shown in the top panel, there are six pinch points on the fidelity surface, implying six phase transition points. In the bottom panel, the contour plot of the ground-state fidelity per lattice site $d(\theta_1,\theta_2)$ on the (θ_1,θ_2) plane is shown, with the truncation dimension up to 4. Therefore, we are able, by evaluating the ground-state fidelity per lattice site, to identify six different phases: the ferromagnetic phase, the rung singlet phase, the staggered dimer phase, the scalar chirality phase, the dominant vector chirality region, and the dominant collinear spin region. Notice that, among six transition points, there are two first-order phase transitions at $\theta \approx -0.40\pi$ and $\theta \approx 0.94\pi$ between ferromagnetic phase and its adjacent phases: the rung singlet phase and the dominant collinear spin region. The remaining four transition points are continuous. These results are in good agreement with the earlier analyses[36,42] based on the exact diagonalization and DMRG. Therefore, the TN algorithm yields reliable results for the two-leg Heisenberg spin ladder with cyclic four-spin exchange. In addition, the ground-state fidelity per lattice site, as a universal marker to detect phase transitions, is able to capture drastic changes of ground-state wave functions around critical points for quantum spin ladders.

Once the ground-state phase diagram is known, we are able to read out local order parameters (if any) from the reduced density matrices for a representative ground-state wave function in a given phase, as advocated in Ref. 28.

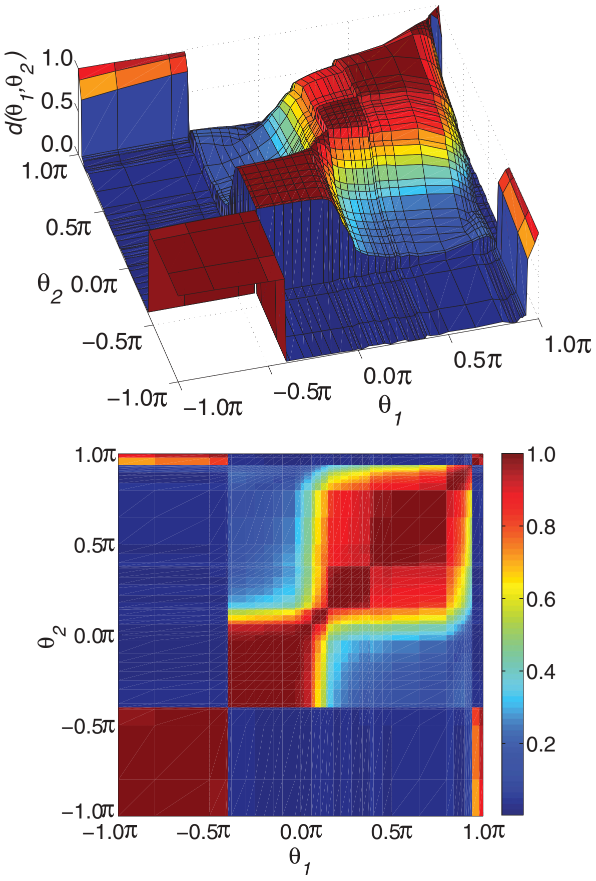

FIG. 9. (Color online) (Top) A two-dimensional fidelity surface embedded in a three-dimensional Euclidean space. (Bottom) The contour plot of the ground-state fidelity per lattice site, $d(\theta_1,\theta_2)$, on the (θ_1,θ_2) plane, for the two-leg Heisenberg spin-$\frac{1}{2}$ ladder with cyclic four-spin exchange. There are six pinch points on the fidelity surface. Therefore, six different phases are identified: the ferromagnetic phase, the rung singlet phase, the staggered dimer phase, the scalar chirality phase, the dominant vector chirality region, and the dominant collinear spin region. The ground-state phase diagram is as follows: the ferromagnetic phase for $-1.06\pi\,(0.94\pi) \lesssim \theta \lesssim -0.40\pi$, the rung singlet phase for $-0.40\pi \lesssim \theta \lesssim 0.06\pi$, the staggered dimer phase for $0.06\pi \lesssim \theta \lesssim 0.15\pi$, the scalar chirality phase for $0.15\pi \lesssim \theta \lesssim 0.38\pi$, the dominant vector chirality region for $0.38\pi \lesssim \theta \lesssim 0.80\pi$, and the dominant collinear spin region for $0.80\pi \lesssim \theta \lesssim 0.94\pi$.

In the ferromagnetic phase, the non-zero-entry structure of the one-site reduced density matrix shows that the $\langle S_{\alpha,i}\rangle$ are the same at all the lattice sites for the two-leg spin ladder. Therefore, the local order parameter is

$$O_F = |\langle\psi_0|S_{\alpha,i}|\psi_0\rangle|. \tag{10}$$

As seen in Fig. 10, $O_F \equiv 0.50$. That is, spins are fully polarized in this phase. In fact, the spin correlations $\langle S_{\alpha,i}\cdot S_{\alpha,i+1}\rangle$ between the nearest-neighbor spins on the legs and the spin correlations $\langle S_{1,i}\cdot S_{2,i}\rangle$ between spins on the rungs are 0.25. The ferromagnetic state minimizes the energy on each plaquette separately for -1.06π $(0.94\pi) \lesssim \theta \lesssim -0.40\pi$.

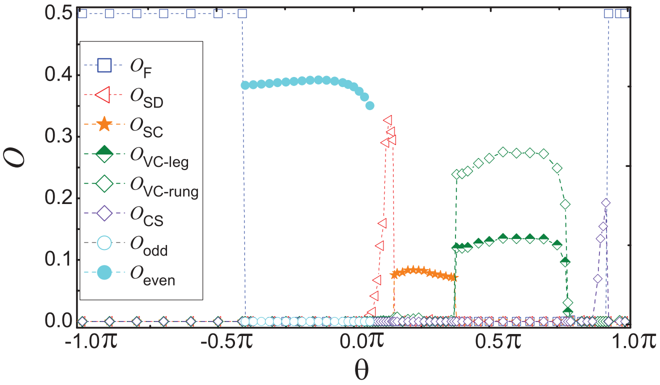

FIG. 10. (Color online) The local order parameters O_F, O_{SD}, O_{SC}, O_{VC}, and O_{CS} in the ferromagnetic phase, the staggered dimer phase, the scalar chirality phase, the dominant vector chirality region, and the dominant collinear spin region and the string order parameters O_{odd}, and O_{even} in the rung singlet phase versus θ, respectively. Note that $O_{\text{odd}} = 0$ and $O_{\text{even}} \neq 0$ for $-0.40\pi \lesssim \theta \lesssim 0.06\pi$, which is characteristic of the rung singlet phase.

In the rung singlet phase, the ground-state wave function may be approximated by the product of local rung singlets. The ground state lacks long-range order in the conventional sense, meaning there is no local order parameter; instead, an exotic order occurs. In fact, the rung singlet phase and the Haldane phase are essentially the same; namely, both are characterized by the string order,[66,67] which may be identified by two distinct string order parameters O_{odd} and O_{even}, as defined in Eq. (6). Actually, the even and odd string order parameters are mutually exclusive: When one is nonzero in a phase, the other vanishes in the same phase. If $O_{\text{odd}} \neq 0$ and $O_{\text{even}} = 0$, then it corresponds to the Haldane phase; if $O_{\text{odd}} = 0$ and $O_{\text{even}} \neq 0$, then it corresponds to the rung singlet phase. As is shown in Fig. 10, our simulation results for O_{odd} and O_{even} for $-0.40\pi \lesssim \theta \lesssim 0.06\pi$ indicate that it is the rung singlet phase.

In the staggered dimer phase, the non-zero-entry structure of the two-site reduced density matrix exhibits a pattern, with the local order parameter as follows,

$$O_{SD} = \tfrac{1}{2}|\langle\psi_0|S_{1,i-1}\cdot S_{1,i} - S_{1,i}\cdot S_{1,i+1} + S_{2,i}\cdot S_{2,i+1} - S_{2,i-1}\cdot S_{2,i}|\psi_0\rangle|. \tag{11}$$

Here, $\langle\psi_0|S_{\alpha,i}\cdot S_{\alpha,i+1}|\psi_0\rangle = \langle\psi_0|S_{1,1}\cdot S_{1,2}|\psi_0\rangle$ if $\alpha + i$ is even; $\langle\psi_0|S_{\alpha,i}\cdot S_{\alpha,i+1}|\psi_0\rangle = \langle\psi_0|S_{2,1}\cdot S_{2,2}|\psi_0\rangle$ if $\alpha + i$ is odd for two degenerate symmetry-breaking ground states in this phase. The ladder is in the staggered dimer phase for $0.06\pi \lesssim \theta \lesssim 0.15\pi$ (cf. Fig. 10).

In the scalar chirality phase, we need to study the non-zero-entry structure of the three-site reduced density matrix. This yields the local order parameter

$$O_{SC} = |\langle\psi_0|S_{1,i}\cdot(S_{2,i}\times S_{1,i+1})|\psi_0\rangle|. \tag{12}$$

It breaks the spatial symmetries and the time-reversal symmetry, but not the internal SU(2) symmetry. The scalar chirality phase lies in $0.15\pi \lesssim \theta \lesssim 0.38\pi$, as seen from Fig. 10.

In the dominant vector chirality region, the non-zero-entry structure of the two-site reduced density matrix yields the local order parameter

$$O_{VC-\text{leg}} = |\langle\psi_0|S_{\alpha,i}\times S_{\alpha,i+1}|\psi_0\rangle|, \tag{13}$$

$$O_{VC-\text{rung}} = |\langle\psi_0|S_{\alpha,i}\times S_{\alpha+1,i}|\psi_0\rangle|. \tag{14}$$

It breaks the spatial symmetries and the time-reversal symmetry. In this phase, the spin correlations are strong between bonds on rungs and legs, but the spin correlations are very weak between diagonal bonds. The order parameter is plotted in Fig. 10, which is nonzero between $0.38\pi \lesssim \theta \lesssim 0.80\pi$.

In the dominant collinear spin region, spins on the same leg exhibit ferromagnetic correlations, while spins on the same rung exhibit antiferromagnetic correlations. The non-zero-entry structure of the one-site reduced density matrix yields the local order parameter

$$O_{CS} = \tfrac{1}{2}|\langle\psi_0|S_{1,i} - S_{2,i}|\psi_0\rangle|. \tag{15}$$

The dominant collinear spin region lies in $0.80\pi \lesssim \theta \lesssim 0.94\pi$.

Therefore, we are able to "derive", by investigating the non-zero-entry structure of the reduced density matrices for representative ground-state wave functions from different phases, the local order parameters for the ferromagnetic phase, the staggered dimer phase, the scalar chirality phase, the dominant vector chirality region, and the dominant collinear spin region, with the local order parameter O_F, O_{SD}, O_{SC}, O_{VC}, and O_{CS} explicitly shown in Fig. 10. In addition, string order parameters O_{odd} and O_{even} are detected in the rung singlet phase, indicating that long-range order is lacking in this phase. The ground-state phase diagram established from the local order parameters coincides with that from the ground-state fidelity per lattice site. That is, the ladder system undergoes four continuous phase transitions at $\theta \approx 0.06\pi$, $\theta \approx 0.15\pi$, $\theta \approx 0.38\pi$, and $\theta \approx 0.80\pi$ and two first-order phase transitions at $\theta \approx -0.40\pi$ and $\theta \approx 0.94\pi$.

D. The ferromagnetic frustrated spin-$\frac{1}{2}$ two-leg ladder

We consider the frustrated spin-$\frac{1}{2}$ two-leg ladder, as depicted in Fig. 11, on an infinite-size lattice. The Hamiltonian takes the form

$$H = H_{\text{leg}} + H_{\text{rung}} + H_{\text{diag}}, \tag{16}$$

where

$$H_{\text{leg}} = J_l \sum_i (\mathbf{S}_{1,i}\cdot\mathbf{S}_{1,i+1} + \mathbf{S}_{2,i}\cdot\mathbf{S}_{2,i+1}), \tag{17}$$

$$H_{\text{rung}} = J_r \sum_i \mathbf{S}_{1,i}\cdot\mathbf{S}_{2,i}, \tag{18}$$

$$H_{\text{diag}} = J_\times \sum_i (\mathbf{S}_{1,i}\cdot\mathbf{S}_{2,i+1} + \mathbf{S}_{2,i}\cdot\mathbf{S}_{1,i+1}). \tag{19}$$

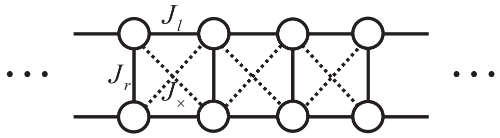

FIG. 11. An infinite-size frustrated spin-$\frac{1}{2}$ two-leg ladder with exchange interaction constants J_l, J_r and $J_\times$ along the leg, rung, and diagonal directions, respectively.

Here, $\mathbf{S}_{\alpha,i}$ ($\alpha = 1,2$) denotes the spin-$\frac{1}{2}$ Pauli operators at site i on the αth leg, J_l is the intrachain coupling between two neighboring spins in each chain, J_r is the rung coupling between two spins on each rung, and $J_\times$ denotes the next-nearest-neighbor interchain coupling.

For this ladder system, we choose J_l to be positive. The system is frustrated with two competing interchain exchanges, the rung coupling J_r and the diagonal coupling $J_\times$. If the coupling parameters J_r and $J_\times$ are varied, the system exhibits two cases: for $J_r > 0$ and $J_\times > 0$, it corresponds to two competing antiferromagnetic interchain couplings;[40,48–58,67–70] for $J_r < 0$ and $J_\times < 0$, it becomes two competing ferromagnetic interchain couplings.[40,41]

We fix the intrachain antiferromagnetic exchange J_l to be unity, and focus on two cases for $J_r < 0$ and $J_\times < 0$: (i) $J_r = -1.6$, and choose $J_\times$ as a control ferromagnetic exchange parameter from $J_\times = -1.00$ to $J_\times = -0.40$; (ii) $J_r = -4.0$, and choose $J_\times$ as a control parameter from $J_\times = -1.00$ to $J_\times = -0.60$. Thus, H_{leg} describes two isotropic Heisenberg chains, H_{rung} and H_{diag} describe frustrated interchain interactions, with two competing interchain ferromagnetic exchanges.

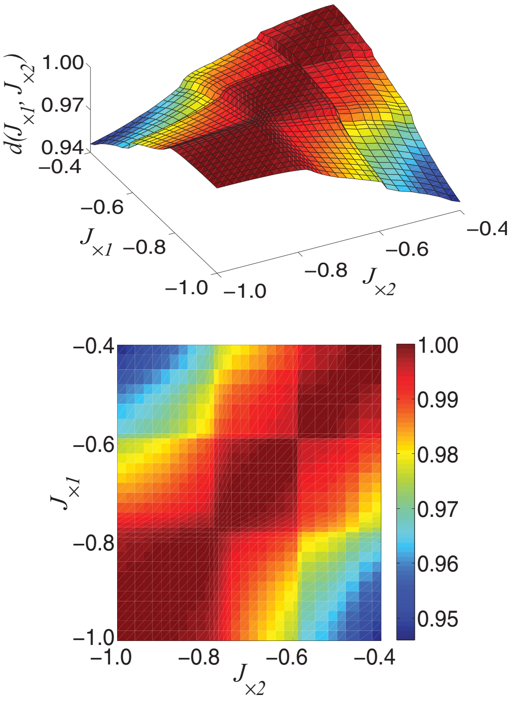

FIG. 12. (Color online) (Top) A two-dimensional fidelity surface embedded in a three-dimensional Euclidean space for the frustrated spin-$\frac{1}{2}$ two-leg ladder with a fixed $J_r = -1.6$ and the diagonal coupling $-1.00 \leqslant J_\times \leqslant -0.40$. Here, the truncation dimension $\mathbb{D}$ is 16. There are two pinch points on the fidelity surface. Therefore, three different phases are identified: the rung singlet phase, the columnar dimer phase, and the Haldane phase. The ground-state phase diagram is as follows: the rung singlet phase for $J_\times < -0.78$, the columnar dimer phase for $-0.78 < J_\times < -0.58$, and the Haldane phase for $J_\times > -0.58$, for a fixed $J_r = -1.6$. (Bottom) The contour plot of the fidelity per lattice site $d(J_{\times 1}, J_{\times 2})$, on the $(J_{\times 1}, J_{\times 2})$ plane, for the frustrated spin-$\frac{1}{2}$ two-leg ladder with a fixed $J_r = -1.6$, and $-1.00 \leqslant J_\times \leqslant -0.40$.

The ground states of the frustrated spin-$\frac{1}{2}$ two-leg ladder with $J_r = -1.6$ and $J_r = -4.0$ for different values of $J_\times < 0$ are computed in the context of the TN representations for an infinite-size spin ladder. As it turns out, the simulation results are in a good agreement with the previous studies from the DMRG method and the analytical RG results in Ref. 40. Here, we focus on the computation of the ground-state fidelity per lattice site, with the truncation dimension $\mathbb{D} = 16$.

In Fig. 12, the ground-state fidelity per lattice site, $d(J_{\times 1}, J_{\times 2})$, is plotted for the frustrated spin-$\frac{1}{2}$ two-leg ladder with a fixed $J_r = -1.6$, and $-1.00 \leqslant J_\times \leqslant -0.40$, with the bond truncation dimension $\mathbb{D} = 16$. In the top panel, we see two pinch points at $(-0.78, -0.78)$ and $(-0.58, -0.58)$, which clearly indicates that there are two phase transitions at $J_{\times c1} \backsimeq -0.78$ and $J_{\times c2} \backsimeq -0.58$, respectively. In the bottom panel, a contour plot is shown for the fidelity per lattice site on the $(J_{\times 1}, J_{\times 2})$ plane. These results are in a good agreement with the earlier analysis based on DMRG and the analytical RG results in Ref. 40.

Therefore, we need to characterize three different phases separated by these two transition points. As advocated in Ref. 28, once the ground-state phase diagram is known, we are able to read out local order parameters (if any) from the reduced density matrices for a representative ground-state wave function in a given phase. As it turns out, three phases are the rung singlet phase, the columnar dimer (CD) phase, and the Haldane phase, respectively. We notice that two continuous phase transitions occur at $J_{\times c1} \backsimeq -0.78$ and $J_{\times c2} \backsimeq -0.58$ between the CD phase and its adjacent phases: the rung singlet phase and the Haldane phase, respectively.

In the CD phase, the non-zero-entry structure of the two-site reduced density matrices yields a local order

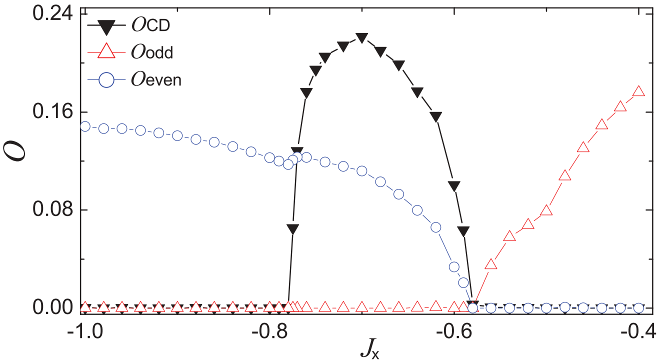

FIG. 13. (Color online) The CD phase local order parameter O_{CD}, and the string order parameters O_{odd} and O_{even}, as a function of $J_\times$ for the frustrated spin-$\frac{1}{2}$ two-leg ladder, respectively, for $J_r = -1.6$. Here, we choose $J_\times$ as a control parameter from $J_\times = -1.00$ to $J_\times = -0.40$. The CD phase is characterized by the local order parameter O_{CD}, whereas the Haldane phase and the rung singlet phase are characterized by the string order parameters O_{odd} and O_{even}, respectively. The system undergoes two continuous phase transitions at $J_{\times c1} \backsimeq -0.78$ and $J_{\times c2} \backsimeq -0.58$, respectively, exhibiting the CD phase for $-0.78 \lesssim J_\times \lesssim -0.58$, the Haldane phase for $J_\times \gtrsim -0.58$, and the rung singlet phase for $J_\times \lesssim -0.78$. The string order parameters are featureless for the CD phase: The even string order parameter O_{even} is nonzero, while the odd string order parameter O_{odd} vanishes. Here, the truncation dimension is $\mathbb{D} = 16$.

parameter,

$$O_{CD} = \tfrac{1}{2}|\langle\psi_0|S_{1,i-1}\cdot S_{1,i} + S_{2,i-1}\cdot S_{2,i} - S_{1,i}\cdot S_{1,i+1} - S_{2,i}\cdot S_{2,i+1}|\psi_0\rangle|. \tag{20}$$

Here, $\langle\psi_0|S_{\alpha,i}\cdot S_{\alpha,i+1}|\psi_0\rangle = \langle\psi_0|S_{1,1}\cdot S_{1,2}|\psi_0\rangle$ if i is odd, $\langle\psi_0|S_{\alpha,i}\cdot S_{\alpha,i+1}|\psi_0\rangle = \langle\psi_0|S_{2,1}\cdot S_{2,2}|\psi_0\rangle$ if i is even, for two degenerate symmetry-breaking ground states in this phase. Indeed, the CD phase is spontaneously dimerized, which breaks translational symmetry (along the chain direction). The CD order is plotted in Fig. 13, while it vanishes in the rung singlet and the Haldane phases.

In the rung singlet phase, rung pairs form singlets, the ground-state wave function can be approximated by the product of local rung singlets. However, the ground state lacks long-range order in the conventional sense; thus, there is no local order parameter. Instead, an exotic order occurs. While in the Haldane phase, the ground-state wave function may be local rung triplets, whose ground states are a direct product of triplet states in each rung, with two spin-$\frac{1}{2}$'s on the rung forming an effective spin-1. In fact, the rung singlet phase and the Haldane phase are essentially the same, for both are characterized by the string order.[66,67] In Fig. 13, we plot the order parameters for different phases, including local order parameter O_{CD} for the CD phase and the string order parameters O_{odd} and O_{even} in Eq. (6) for the rung singlet phase and the Haldane phase, as a function of $J_\times$ for the frustrated spin-$\frac{1}{2}$ two-leg ladder, with $J_r = -1.6$. In the absence of a local order parameter, it is known that, for $O_{\text{odd}} \neq 0$ and $O_{\text{even}} = 0$, it corresponds to the Haldane phase; for $O_{\text{odd}} = 0$ and $O_{\text{even}} \neq 0$, it corresponds to the rung singlet phase. Therefore, the rung singlet phase lies in $J_\times \lesssim -0.78$, the Haldane phase lies in $J_\times \gtrsim -0.58$, and the CD phase lies in $-0.78 \lesssim J_\times \lesssim -0.58$. Notice that, in the CD phase, the even string order parameter O_{even} is nonzero, while the odd string order parameter O_{odd} vanishes. However, the even string order parameter O_{even} is nonzero in both the CD phase and the rung singlet phase; thus, it is unable to distinguish them. As we see, the ground-state phase diagram established from both the local order parameter and the string order parameters coincides with that from the ground-state fidelity per lattice site. That is, the frustrated spin-$\frac{1}{2}$ two-leg ladder system undergoes two continuous phase transitions at $J_{\times c1} \backsimeq -0.78$ and $J_{\times c2} \backsimeq -0.58$ for a fixed $J_r = -1.6$, and $-1.00 \leqslant J_\times \leqslant -0.40$.

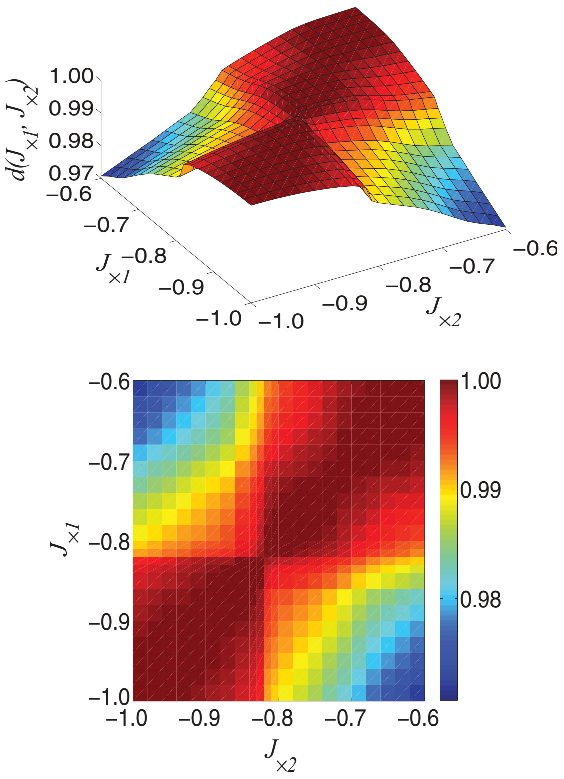

FIG. 14. (Color online) The ground-state fidelity per lattice site, $d(J_{\times 1}, J_{\times 2})$, for the frustrated spin-$\frac{1}{2}$ two-leg ladder with a fixed $J_r = -4.0$, and $-1.00 \leqslant J_\times \leqslant -0.60$. Here, the truncation dimension $\mathbb{D}$ is 16. (Top) In a three-dimensional Euclidean space, the two-dimensional fidelity surface clearly indicates that there is a phase transition point, as a pinch point occurs at $J_{\times c3} \backsimeq -0.81$. (Bottom) The contour plot of the fidelity per lattice site $d(J_{\times 1}, J_{\times 2})$, on the $(J_{\times 1}, J_{\times 2})$ plane, for the frustrated spin-$\frac{1}{2}$ two-leg ladder with a fixed $J_r = -4.0$, and $-1.00 \leqslant J_\times \leqslant -0.60$ with the truncation dimension $\mathbb{D} = 16$.

In Fig. 14, the ground-state fidelity per lattice site, $d(J_{\times 1}, J_{\times 2})$, is plotted for the frustrated spin-$\frac{1}{2}$ two-leg ladder with $J_r = -4.0$, and $-1.00 \leqslant J_\times \leqslant -0.60$. Here, the truncation dimension $\mathbb{D}$ is 16. In a three-dimensional Euclidean space, the two-dimensional fidelity surface clearly indicates that there exists a phase transition point, shown as a pinch point at $(-0.81, -0.81)$ in the top panel. The contour plot of the fidelity per lattice site $d(J_{\times 1}, J_{\times 2})$ on the $(J_{\times 1}, J_{\times 2})$ plane is shown in the bottom panel. Hence, the computation of the ground-state fidelity per lattice site enables us to conclude that a continuous phase transition takes place at $J_{\times c3} \simeq -0.81$, which is in a good agreement with the earlier results from Ref. 40.

In Fig. 15, we plot the local order parameter O_{CD} for the CD phase, as defined by Eq. (20), and the string order parameters

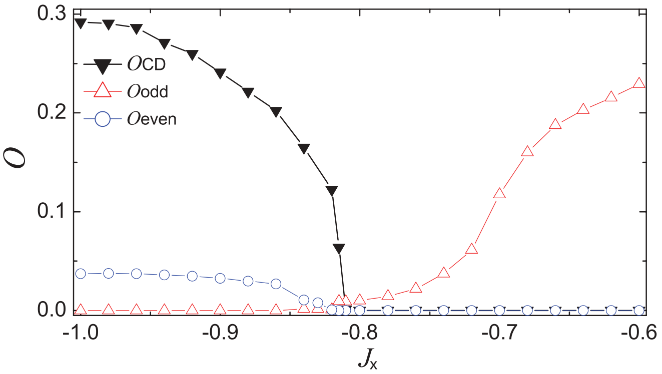

FIG. 15. (Color online) The local order parameter O_{CD} for the CD phase, and the string order parameters O_{odd} and O_{even} for the Haldane phase, as a function of $J_\times$ for the frustrated spin-$\frac{1}{2}$ two-leg ladder with $J_r = -4.0$ and $-1.00 \leqslant J_\times \leqslant -0.60$. The system undergoes a continuous phase transition at $J_{\times c3} \backsimeq -0.81$, exhibiting the CD phase for $J_\times \lesssim -0.81$, and the Haldane phase for $J_\times \gtrsim -0.81$. Note that, for the CD phase, the even string order parameter $O_{\text{even}} \neq 0$, while the odd string order parameter $O_{\text{odd}} = 0$. Here, the truncation dimension is $\mathbb{D} = 16$.

O_{odd} and O_{even} for the Haldane phase, as defined by Eq. (6), as a function of $J_\times$ for the frustrated spin-$\frac{1}{2}$ two-leg ladder, with $J_r = -4.0$. Similar to the $J_r = -1.6$ case, the Haldane phase lies in $J_\times \gtrsim -0.81$ and the CD phase lies in $-1.00 \lesssim J_\times \lesssim -0.81$ for $J_r = -4.0$. Here, for the CD phase, we find that the even string order parameter O_{even} is nonzero, while the odd string order parameter O_{odd} vanishes. Again, the ground-state phase diagram established from the order parameters coincides with that from the ground-state fidelity per lattice site. That is, the frustrated spin-$\frac{1}{2}$ two-leg ladder system undergoes a continuous phase transition at $J_{\times c3} \backsimeq -0.81$ for $J_r = -4.0$, and $-1.00 \leqslant J_\times \leqslant -0.40$.

V. CONCLUSIONS

We have developed an efficient TN algorithm to compute ground-state wave functions for infinite-size quantum spin ladders. For all the models investigated, the phase transition points detected by means of both the ground-state fidelity per lattice site and the order parameters coincide with each other and are consistent with those from the ED and/or DMRG. For the two-leg Heisenberg spin ladder with staggering dimerization, we compare the ground-state energies with those from both the ED and the DMRG and find that our results are comparable to the previous DMRG results. Indeed, the TN algorithm even outperforms the DMRG in some specific situations for a quite small truncation dimension. Unfortunately, except for the two-leg Heisenberg spin ladder with staggering dimerization, no numerical DMRG results for the ground-state energy for infinite-size spin ladders are available to be compared with. Given that, for a TN algorithm, a larger truncation dimension yields a more accurate result, one may anticipate that the TN algorithm outperforms other approaches, since the computational cost is relatively lower.

In addition, it is worthwhile to mention that, similar to a gapless phase, a gapful phase with a finite but quite small gap, such as the scalar chirality, the vector chirality phase, and the Haldane phase, as expected, are more difficult to simulate than a gapful phase with a larger gap, such as the ferromagnetic phase. However, our algorithm still converges well in these phases. In fact, the ground-state energy relative error between the truncation dimensions $\mathbb{D} = 6$ and $\mathbb{D} = 8$ reaches up to 10^{-4} for these phases. In comparison, for the ferromagnetic phase, it reaches up to 10^{-6}. Another point we would like to mention is that, even if we choose the truncation dimension $\mathbb{D}$ to be as small as 4, we are still able to detect all the relevant phase transition points quite accurately, compared to those with larger truncation dimensions. As a typical example, for the ferromagnetic frustrated spin-$\frac{1}{2}$ two-leg ladder model, no significant shift is observed for the phase transition points detected with $\mathbb{D} = 4$, compared to those detected with $\mathbb{D} = 16$. In this sense, it is sufficient to simulate a spin-ladder system with a relatively small truncation dimension for the detection of phase transition points in terms of the ground-state fidelity per lattice site.

Our investigation lends further support to the observation that the ground-state fidelity per lattice site is able to characterize critical phenomena in quantum many-body systems. It also demonstrates that the developed TN algorithm for spin ladders makes it possible to efficiently compute the ground-state fidelity per lattice site. This is systematically tested for the two-leg and three-leg Heisenberg spin ladders with staggering dimerization, the two-leg Heisenberg spin ladder with cyclic four-spin exchange, and the ferromagnetic frustrated two-leg ladder. Our simulation results clearly indicate that the TN algorithm yields reliable results for spin-ladder systems. In addition, the ground-state fidelity per lattice site, a universal marker to detect phase transitions, shows its capability to capture drastic changes of ground-state wave functions around phase transition points for quantum spin-ladder systems. Last but not least, we are able to "derive" local order parameters (if any) from the reduced density matrices for a representative ground-state wave function in a given phase and characterize a phase without any long-range order in terms of the string order parameters.

ACKNOWLEDGMENTS

We thank Sam Young Cho, Bing-Quan Hu, Bo Li, Hong-Lei Wang, Ai-Min Chen, and Jian-Hui Zhao for enlightening discussions. This work is supported in part by the National Natural Science Foundation of China (Grants No. 11174375 and No. 11104362). S.H.L., Q.Q.S., Y.H.S., J.H.L., and Y.W.D. are supported by the Fundamental Research Funds for the Central Universities (Project No. CDJXS11102213), by Chongqing University Postgraduates' Science and Innovation Fund (Project No. 200911C1A0060322), and by the Innovative Talent Funds for Project 985 (Projects No. WLYJSBJRCGR201103 and No. WLYJSBJRCGR201104).

---

[1] M. Fannes, B. Nachtergaele, and R. F. Werner, Commun. Math. Phys. **144**, 443 (1992); J. Funct. Anal. **120**, 511 (1994); S. Östlund and S. Rommer, Phys. Rev. Lett. **75**, 3537 (1995).

[2] D. Perez-Garcia, F. Verstraete, M. M. Wolf, and J. I. Cirac, Quantum Inf. Comput. **7**, 401 (2007).

[3] F. Verstraete, D. Porras, and J. I. Cirac, Phys. Rev. Lett. **93**, 227205 (2004).

[4] G. Vidal, Phys. Rev. Lett. **91**, 147902 (2003); **93**, 040502 (2004).

[5] G. Vidal, Phys. Rev. Lett. **98**, 070201 (2007).

[6] F. Verstraete and J. I. Cirac, arXiv:cond-mat/0407066.

[7] V. Murg, F. Verstraete, and J. I. Cirac, Phys. Rev. A **75**, 033605 (2007).

[8] J. Jordan, R. Orús, G. Vidal, F. Verstraete, and J. I. Cirac, Phys. Rev. Lett. **101**, 250602 (2008).

[9] P. Pippan, S. R. White, and H. G. Evertz, Phys. Rev. B **81**, 081103(R) (2010).

[10] Q.-Q. Shi and H.-Q. Zhou, J. Phys. A: Math. Theor. **42**, 272002 (2009).

[11] B. Pirvu, F. Verstraete, and G. Vidal, Phys. Rev. B **83**, 125104 (2011).

[12] H. C. Jiang, Z. Y. Weng, and T. Xiang, Phys. Rev. Lett. **101**, 090603 (2008).

[13] J. Haegeman, J. I. Cirac, T. J. Osborne, I. Pižorn, H. Verschelde, and F. Verstraete, Phys. Rev. Lett. **107**, 070601 (2011).

[14] B. Li, S.-H. Li, and H.-Q. Zhou, Phys. Rev. E **79**, 060101(R) (2009).

[15] L. Wang, Y.-J. Kao, and A. W. Sandvik, Phys. Rev. E **83**, 056703 (2011).

[16] P. C. Chen and M.-F. Yang, Phys. Rev. B **82**, 180510(R) (2010).

[17] C.-Y. Huang and F.-L. Lin, arXiv:0911.4670.

[18] H.-Q. Zhou and J. P. Barjaktarević, J. Phys. A: Math. Theor. **41**, 412001 (2008).

[19] H.-Q. Zhou, J.-H. Zhao, and B. Li, J. Phys. A: Math. Theor. **41**, 492002 (2008).

[20] H.-Q. Zhou, arXiv:0704.2945.

[21] H.-Q. Zhou, R. Orús, and G. Vidal, Phys. Rev. Lett. **100**, 080601 (2008).

[22] J.-H. Zhao, H.-L. Wang, B. Li, and H.-Q. Zhou, Phys. Rev. E **82**, 061127 (2010).

[23] H.-L. Wang, J.-H. Zhao, B. Li, and H.-Q. Zhou, J. Stat. Mech. (2011) L10001.

[24] P. Zanardi and N. Paunković, Phys. Rev. E **74**, 031123 (2006).

[25] P. Zanardi, M. Cozzini, and P. Giorda, J. Stat. Mech. (2007) L02002; N. Oelkers and J. Links, Phys. Rev. B **75**, 115119 (2007); M. Cozzini, R. Ionicioiu, and P. Zanardi, *ibid.* **76**, 104420 (2007); L. Campos Venuti and P. Zanardi, Phys. Rev. Lett. **99**, 095701 (2007); T. Liu, Y.-Y. Zhang, Q.-H. Chen, and K.-L. Wang, Phys. Rev. A **80**, 023810 (2009).

[26] W.-L. You, Y.-W. Li, and S.-J. Gu, Phys. Rev. E **76**, 022101 (2007); S. J. Gu, H. M. Kwok, W. Q. Ning, and H. Q. Lin, Phys. Rev. B **77**, 245109 (2008); M. F. Yang, *ibid.* **76**, 180403(R) (2007); Y. C. Tzeng and M. F. Yang, Phys. Rev. A **77**, 012311 (2008); J. O. Fjærestad, J. Stat. Mech.: Theory Exp. (2008) P07011; J. Sirker, Phys. Rev. Lett. **105**, 117203 (2010).

[27] M. M. Rams and B. Damski, Phys. Rev. Lett. **106**, 055701 (2011).

[28] H.-Q. Zhou, arXiv:0803.0585.

[29] E. Dagotto and T. M. Rice, Science **271**, 618 (1996).

[30] T. Giamarchi, *Quantum Physics in One Dimension* (Oxford University Press, Oxford, 2004).

[31] N. Flocke, Phys. Rev. B **56**, 13673 (1997).

[32] G. Y. Chitov, B. W. Ramakko, and M. Azzouz, Phys. Rev. B **77**, 224433 (2008).

[33] S. J. Gibson, R. Meyer, and G. Y. Chitov, Phys. Rev. B **83**, 104423 (2011).

[34] M. A. Martin-Delgado, J. Dukelsky, and G. Sierra, Phys. Lett. A **250**, 430 (1998).

[35] J. Almeida, M. A. Martin-Delgado, and G. Sierra, Phys. Rev. B **76**, 184428 (2007); **77**, 094415 (2008); J. Phys. A **41**, 485301 (2008).

[36] J.-L. Song, S.-J. Gu, and H.-Q. Lin, Phys. Rev. B **74**, 155119 (2006).

[37] Y. Honda and T. Horiguchi, arXiv:cond-mat/0106426.

[38] T. Hikihara, T. Momoi, and X. Hu, Phys. Rev. Lett. **90**, 087204 (2003).

[39] K. Hijii, S. Qin, and K. Nomura, Phys. Rev. B **68**, 134403 (2003).

[40] T. Hikihara and O. A. Starykh, Phys. Rev. B **81**, 064432 (2010).

[41] N. Zhu, X. Wang, and C. Chen, Phys. Rev. B **63**, 012401 (2000).

[42] A. Läuchli, G. Schmid, and M. Troyer, Phys. Rev. B **67**, 100409(R) (2003).

[43] K. Hijii and K. Nomura, Phys. Rev. B **65**, 104413 (2002).

[44] Ö. Legeza, G. Fáth, and J. Sólyom, Phys. Rev. B **55**, 291 (1997); T. Hikihara and A. Furusaki, *ibid.* **63**, 134438 (2001); J.-B. Fouet, F. Mila, D. Clarke, H. Youk, O. Tchernyshyov, P. Fendley, and R. M. Noack, *ibid.* **73**, 214405 (2006); J. S. Meyer and K. A. Matveev, J. Phys.: Condens. Matter **21**, 023203 (2009); D. N. Sheng, O. I. Motrunich, S. Trebst, E. Gull, and M. P. A. Fisher, Phys. Rev. B **78**, 054520 (2008).

[45] S. P. Strong and A. J. Millis, Phys. Rev. Lett. **69**, 2419 (1992).

[46] X. Wang and L. Yu, Phys. Rev. Lett. **84**, 5399 (2000).

[47] I. Maruyama, T. Hirano, and Y. Hatsugai, Phys. Rev. B **79**, 115107 (2009).

[48] M. P. Gelfand, Phys. Rev. B **43**, 8644 (1991); I. Bose and S. Gayen, *ibid.* **48**, 10653 (1993); Y. Xian, *ibid.* **52**, 12485 (1995); H. Kitatani and T. Oguchi, J. Phys. Soc. Jpn. **65**, 1387 (1996).

[49] Weihong Zheng, V. Kotov, and J. Oitmaa, Phys. Rev. B **57**, 11439 (1998).

[50] D. Allen, F. H. L. Essler, and A. A. Nersesyan, Phys. Rev. B **61**, 8871 (2000).

[51] E. H. Kim, G. Fáth, J. Sólyom, and D. J. Scalapino, Phys. Rev. B **62**, 14965 (2000).

[52] A. Honecker, F. Mila, and M. Troyer, Eur. Phys. J. B **15**, 227 (2000).

[53] X. Q. Wang, Mod. Phys. Lett. B **14**, 327 (2000).

[54] G. Fáth, Ö. Ligeza, and J. Sólyom, Phys. Rev. B **63**, 134403 (2001).

[55] T. Hakobyan, J. H. Hetherington, and M. Roger, Phys. Rev. B **63**, 144433 (2001).

[56] M. Tsuchiizu and A. Furusaki, Phys. Rev. Lett. **88**, 056402 (2002).

[57] A. A. Nersesyan and A. M. Tsvelik, Phys. Rev. B **67**, 024422 (2003).

[58] M. Nakamura, Physica B **329-333**, 1000 (2003).

[59] Y. Mizuno, T. Tohyama, and S. Maekawa, J. Low. Temp. Phys. **117**, 389 (1999).

[60] M. Azuma, Z. Hiroi, M. Takano, K. Ishida, and Y. Kitaoka, Phys. Rev. Lett. **73**, 3463 (1994).

[61] M. Matsuda, K. Katsumata, R. S. Eccleston, S. Brehmer, and H.-J. Mikeska, Phys. Rev. B **62**, 8903 (2000).

[62] T. Imai, K. R. Thurber, K. M. Shen, A. W. Hunt, and F. C. Chou, Phys. Rev. Lett. **81**, 220 (1998).

[63] S. R. White, Phys. Rev. Lett. **69**, 2863 (1992); Phys. Rev. B **48**, 10345 (1993).

[64] If no translational symmetry is spontaneously broken in a translational invariant system under one-site shifts, it seems to be natural to choose a unit cell consisting of just two tensors (one for each leg in a two-leg spin ladder). However, some phases, such as the staggered dimmer phase, the scalar chirality phase, the dominant vector chirality phase, and the columnar dimer phase, are not well described with such a choice of the unit cell. Instead, regardless of breaking or not of the translational symmetry for an infinite-size two-leg spin-ladder system, the unit cell consisting of four tensors, as we have chosen, is enough to accommodate all the phases for the spin-ladder systems we discussed here.

[65] P. Debabrata and K. P. Swapan, J. Phys.: Condens. Matter **19**, 172201 (2007).

[66] M. den Nijs and K. Rommelse, Phys. Rev. B **40**, 4709 (1989); S. R. White, *ibid.* **53**, 52 (1996); E. H. Kim, Ö. Ligeza, and J. Sólyom, *ibid.* **77**, 205121 (2008); M. Nakamura and S. Todo, Phys. Rev. Lett. **89**, 077204 (2002); G. Fáth, Ö. Legeza, and J. Sólyom, Phys. Rev. B **63**, 134403 (2001).

[67] H.-H. Hung, C. D. Gong, Y.-C. Chen, and M.-F. Yang, Phys. Rev. B **73**, 224433 (2006).

[68] O. A. Starykh and L. Balents, Phys. Rev. Lett. **93**, 127202 (2004).

[69] M. Tsuchiizu and A. Furusaki, Phys. Rev. B **69**, 035103 (2004).

[70] G.-H. Liu, H.-L. Wang, and G.-S. Tian, Phys. Rev. B **77**, 214418 (2008).